High-Performance Silicon Photonics Using Heterogeneous Integration

Chao Xiang , *Member, IEEE*, Warren Jin, Duanni Huang, *Member, IEEE*, Minh A. Tran , *Member, IEEE*,
Joel Guo , Yating Wan , Weiqiang Xie, Geza Kurczveil , *Member, IEEE*, Andrew M. Netherton,
Di Liang , *Senior Member, IEEE*, Haisheng Rong , *Senior Member, IEEE*,
and John E. Bowers , *Life Fellow, IEEE*

(Invited Paper)

Abstract—The performance of silicon photonic components and integrated circuits has improved dramatically in recent years. As a key enabler, heterogeneous integration not only provides the optical gain which is absent from native Si substrates and enables complete photonic functionalities on chip, but also lays the foundation of versatile integrated photonic device performance engineering. This paper reviews recent progress of high-performance silicon photonics using heterogeneous integration, with emphasis on ultra-low-loss waveguides, single-wavelength lasers, comb lasers, and photonic integrated circuits including optical phased arrays for LiDAR and optical transceivers for datacenter interconnects.

Index Terms—Silicon photonics, lasers, photonic integration.

I. Introduction

FOR the past fifty years, most telecom, datacom and sensor systems have relied on individual optical components, such as lasers, modulators and photodetectors [1]. Recently, integrated photonics has been commercialized due to its advantages in terms of size, weight, cost and power consumption [2], [3]. The performance of photonic integrated circuits (PICs) is largely determined by the selection of the integration platform. Silicon photonics leverages mature CMOS facilities for high-yield, low-cost manufacturing of photonic components and may have an intrinsic advantage over the III-V-based devices due to the availability of low loss and compact waveguides. Silicon photonic modulators, photodetectors and passive devices are available through monolithic silicon-on-insulator (SOI) waveguide based structures. Heterogeneous integration using bonded III-V active materials onto SOI provide optical gain and thus enables lasers and amplifiers, expanding the complexity and improving the performance of PICs [4].

Heterogeneous integration allows the selection of optical materials for the best achievable on-chip performance. For example, in addition to quantum wells (QWs), III-V active materials are now supplemented with quantum dots (QDs) for wide gain bandwidth and high temperature operation [5]. On the passive waveguide side, ultra-low loss silicon nitride (Si_3N_4) waveguides are being integrated for a wide variety of applications and heterogeneous device performance optimization [6]–[8]. As an example, semiconductor laser frequency noise can be reduced by 50 dB by self injection locking (SIL) the laser to ultra-low loss Si_3N_4 waveguides [9]. A wide range of available materials from group IV, III-V and II-VI semiconductors to dielectric, ferroelectric, piezoelectric, and magnetic materials can be integrated [10], [11]. The integration approach can be die-to-wafer, wafer-to-wafer bonding [12] or micro-transfer-printing [13]. It can also be combined with heteroepitaxial growth to further reduce the cost and improve the integration versatility [14], [15].

Photonic integrated circuits with dense integration of lasers, modulators and other devices are evolving rapidly from proof-of-concept demonstrations to products shipping million units per year [16]. The elimination of chip-to-chip coupling loss and availability of on-chip gain from heterogeneous integration expanded its application scenarios from optical transceivers to sensors, such as gyroscopes and LiDAR [17], [18]. The high integration level also results in high energy efficiency. Heterogeneous integration with co-packaged silicon photonics and electronics is the key towards future petabyte-per-second bandwidth network switches in datacenters [19]. The scalability of heterogeneous integration is naturally compatible with silicon photonics using CMOS facilities. Industry-standard 300-mm-diameter or 200-mm-diameter Si substrates promise the scalable production of heterogeneous PICs with similar performance, but at orders of magnitude lower cost and higher manufacturing scale [16], [20].

Chao Xiang, Warren Jin, Joel Guo, Yating Wan, Weiqiang Xie, Andrew M. Netherton, and John E. Bowers are with the Department of Electrical and Computer Engineering, University of California, Santa Barbara, CA 93106 USA (e-mail: cxiang@ece.ucsb.edu; warren@ece.ucsb.edu; joelguo@ucsb.edu; yatingwan@ucsb.edu; weiqiangxie@ucsb.edu; anetherton@ece.ucsb.edu; bowers@ece.ucsb.edu).

Geza Kurczveil and Di Liang are with Hewlett Packard Labs, Hewlett Packard Enterprise, Milpitas, CA 95035 USA (e-mail: geza.kurczveil@hpe.com; di.liang@ieee.org).

Duanni Huang and Haisheng Rong are with Intel Corporation, Santa Clara, CA 95054 USA (e-mail: duanni.huang@intel.com; haisheng.rong@intel.com).

Minh A. Tran is with Nexus Photonics, Goleta, CA 93117 USA (e-mail: minhtrananh@gmail.com).
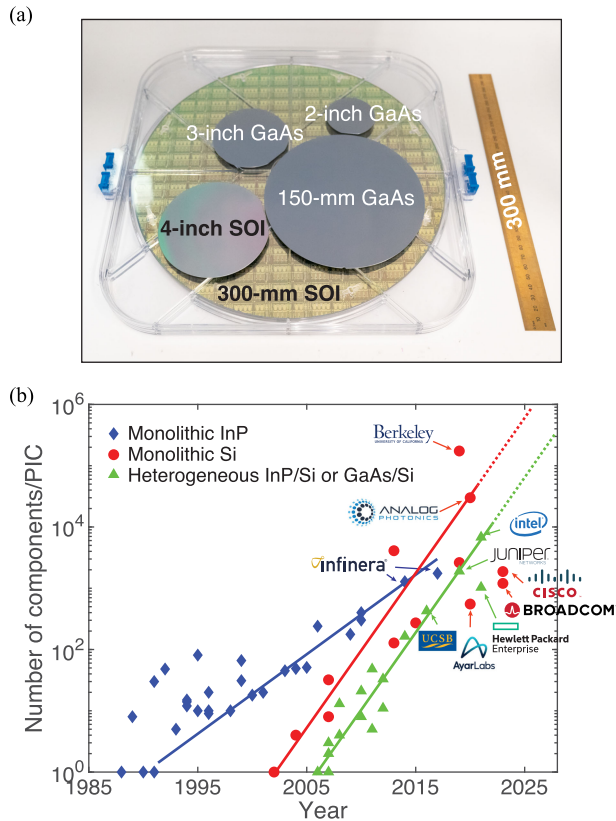
(a)

(b)

Fig. 1. (a) Wafer size comparison of a 300-mm SOI wafer with smaller-sized GaAs and SOI wafers. (b) The number of photonic components integrated on a single PIC over time for three photonic integration platforms [19].

A comparison of the wafer sizes is shown in Fig. 1(a). Industry-standard 300-mm-diameter SOI wafers offer a high device throughput. Indium phosphide (InP) substrate PICs are commonly restricted to 4-inch or smaller. Gallium arsenide (GaAs) substrates PICs are making a transition from small size (2-inch, 3-inch) to 150-mm substrates, but its average material cost is still significantly higher than 300-mm Si substrates. The integration level of monolithic and heterogeneous silicon photonics is growing at similar pace with increasing number of components integrated on a single PIC (Fig. 1(b)) [19]. With the addition of on-chip lasers and amplifiers, the integration level and device scale of heterogeneous Si PICs are projected to exceed that of monolithic Si PICs without lasers.

This paper is organized as follows. We start with introducing the most recent results in high-performance silicon photonic devices using heterogeneous integration (Section II). This section starts with the developments of ultra-low loss silicon and silicon nitride waveguides, which is a key motivation of silicon photonics and also forms the basis of several key performance optimizations for heterogeneous integrated devices. This section then discusses progress in lasers with the unique silicon photonic devices enabled by heterogeneous integration, including single-wavelength lasers and comb lasers. We highlight the developments in both gain materials and laser passive cavity. We then showcase the recent representative photonic integrated circuits, showing the improving integration scale and future integration perspectives with electronics (Section III). In Section IV, we

discuss the advantages of commercializing heterogeneous silicon photonic circuits in datacenters for co-packaged optics and present an exemplary heterogeneous silicon photonic transceiver from an Intel 300-mm CMOS fab, which achieved a total of 260 Gbps data rate on a single wavelength. Finally in Section V, we provide a summary and future perspectives on heterogeneous integration in silicon photonics.

II. SILICON PHOTONIC DEVICES

Heterogeneous integration allows performance optimization for both passive and active devices. This section focuses on the recent progress of ultra-low loss waveguides and heterogeneous integrated lasers on Si.

A. Ultra-Low Loss Waveguides

The availability of low-loss integrated photonic waveguides is critical, not only for reducing component insertion losses as the scale and complexity of integrated photonic circuits increases, but also for enabling emerging microresonator-based technologies, such as as on-chip soliton microcombs [23] and ultra-narrow linewidth integrated lasers [24], whose performance improves with increasing cavity Q-factor [25], [26] (i.e decreasing propagation loss).

Thanks to decades-long development of CMOS technology for the microelectronics industry, silicon, silicon dioxide, and silicon nitride thin films are widely available in foundries for use as high quality waveguide core and cladding material on wafers up to 300 mm in diameter. Fig. 2 compares the achieved loss in waveguide platforms compatible with heterogeneous integration. Compared to > 1 dB/cm waveguide loss in GaAs or InP waveguides, typical silicon waveguide loss is on the order of 0.1 dB/cm to 1 dB/cm. Silicon waveguide losses are largely dominated by sidewall scattering losses and can be reduced by reducing etch depth and increasing waveguide width. Indeed, 5 dB/m loss was achieved in a 500 nm thick device layer at 56 nm etch depth and 8 μm width in multi-mode silicon rib waveguides [27]. It needs to be noted that the selection of 56 nm is based on the equipped etch depth monitor at UCSB Nanofab facility which gives an accurate etch depth control. The etch depth can be varied as long as the shallow etch depth is precisely controlled and supports highly confined mode with reduced mode interaction with waveguide sidewalls. The 500-nm thickness of Si instead of 220 nm that is widely used for SOI wafers is favored here for both low loss and also possible integration with heterogeneous III-V lasers. Additional improvements of photoresist reflow and optimized etch chemistry enabled 3 dB/m propagation loss at a deeper etch depth of 190 nm for the same device layer thickness and waveguide width [22]. Moreover, silicon waveguides can be efficiently coupled to silicon nitride waveguides on the same platform [28]. Recent progress of silicon nitride waveguides have demonstrated waveguides loss ranging from 0.1 dB/cm to 0.001 dB/cm (0.1 dB/m), using CMOS-ready processing techniques. A recent publication has demonstrated as low as 0.1 dB/m loss using high-temperature processing within a CMOS foundry [9]. However, reducing the thermal budget for back-end processing (high temperature annealing to reduce hydrogen absorption) is desirable to facilitate
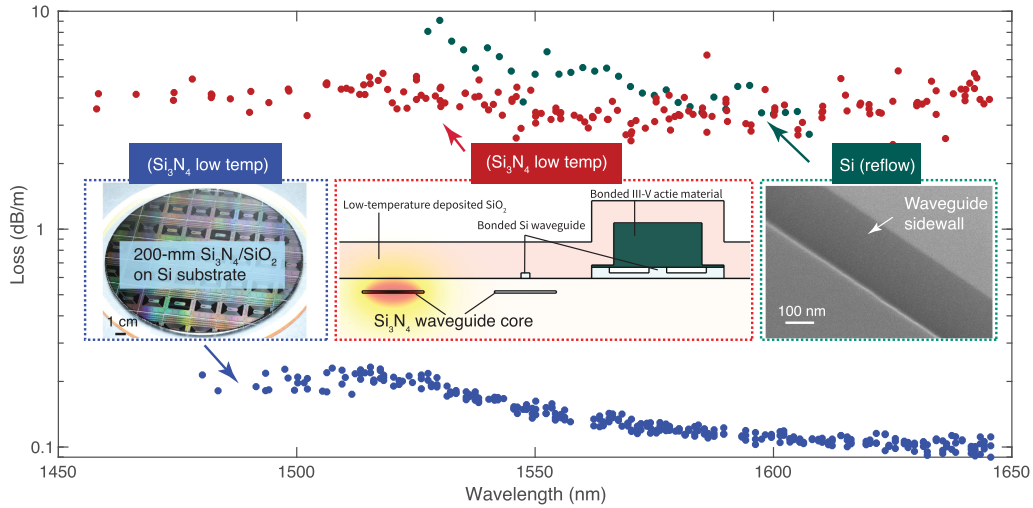
Fig. 2. Comparison of achieved waveguide loss for waveguide platforms compatible with heterogeneous integration. Propagation loss of 0.1 dB/m has been achieved in Si_3N_4 subject to high temperature annealing [9], while around 3 dB/m has been demonstrated within the thermal budget of heterogeneous integration using either a deuterated, low-temperature top-oxide-cladded single-mode Si_3N_4 waveguides [21], or multi-mode silicon waveguides [22].

integration with III-V materials. For this case, a low temperature, deuterated, silicon dioxide top cladding was developed with demonstrated loss of 3 dB/m [21] and has been successfully integrated into heterogeneous lasers [8], [29].

B. Single-Wavelength Lasers

Single wavelength lasers are important in applications including optical interconnects, optical communications, sensing etc. Single-wavelength lasers require wavelength-selective filters. Heterogeneous integration provides versatile flexibility of using silicon-based cavity for the single-wavelength selection. Grating-based DFB (distributed feedback) or DBR (distributed Bragg reflector) lasers offer the ease of operation, while ring-resonator-based lasers can enable a widely tunable range and greater laser noise reduction.

An advantage of heterogeneous III-V/Si lasers is the availability of on-chip Si mirrors or Si facets as the laser mirror. The degradation of cleaved facets in monolithic III-V lasers can thus be eliminated due to the excellent robustness of passive Si-based mirrors. Fig. 3(a) shows a scanning electron microscope (SEM) image of heterogeneous III-V/Si lasers with on-chip Si loop mirrors as the laser reflectors. III-V/Si monitor photodetectors (PDs) can be included to enable and expedite wafer-scale laser screening and testing.

1) Grating-Based III-V/Si Lasers: Si waveguide Bragg grating can offer excellent single-wavelength filtering, thus enabling III-V/Si-based DFB lasers and DBR lasers. A narrow-band grating response together with high side lobe suppression ratio is required for high-performance grating-based single-wavelength lasers, since it directly impacts the laser linewidth and laser side mode suppression ratio (SMSR) [2]. Si offers excellent low loss waveguide which can form high-Q and narrow-band Si waveguide Bragg filters. In applications where high-power and narrow linewidth is preferred, e.g externally modulated lasers

and sensing applications, the heterogeneous III-V/Si DFB or DBR lasers offer excellent performance.

For III-V/Si DFB lasers, the grating is etched on the Si layer under the III-V gain mesa area. The DFB grating can be etched on the top, on the sidewall of the rib waveguide core, or on the rib section of the Si rib waveguide. For a long III-V/Si DFB laser targeting high output power, the grating κ needs to be kept small to lower the grating κL_g value and consequently, a narrow filter bandwidth for single mode selectivity. The SEM image of the side grating etched on the Si waveguide rib and an image of the InP/Si QW DFB laser array are shown in the inset Fig. 3(b).

The maximum output power of a 1.2-mm long InP/Si DFB laser is over 20 mW. The optical spectrum in Fig. 3(b) shows over 67 dB SMSR due to the excellent mode selectivity provided by the side hole Si rib grating. This laser alone, or integrated together with a semiconductor optical amplifier, could be the pump source for on-chip nonlinear applications through heterogeneous integration with nonlinear materials including AlGaAs, LiNbO $_3$ (lithium niobate) or Si_3 N_4.

Another type of Bragg grating-based laser is a DBR laser. While DFB lasers are limited in grating length by the active III-V section length, DBR lasers have the potential to include an ultra-long external cavity. Low-loss Si could enable a long external cavity without significantly increasing the cavity loss. As a result, it offers more potential for laser performance engineering.

Fig. 3(c) shows an image of heterogeneous III-V/Si extended DBR (E-DBR) laser array that contains twelve lasers [31]. The gratings are based on shallow-etched (56 nm etch depth) Si rib waveguide. The grating κ is controlled through the gap distance between the etch holes and Si rib waveguide core. For ultra small κ values, a long grating length is possible for a fixed target κL_g value. A 15-mm long Bragg grating is designed to maximize the linewidth reduction ratio through passive-active cavity integration. The fundamental linewidth of such external cavity based laser is $\Delta v = \Delta v_0/(1 + A + B)^2$, where Δv_0 is the
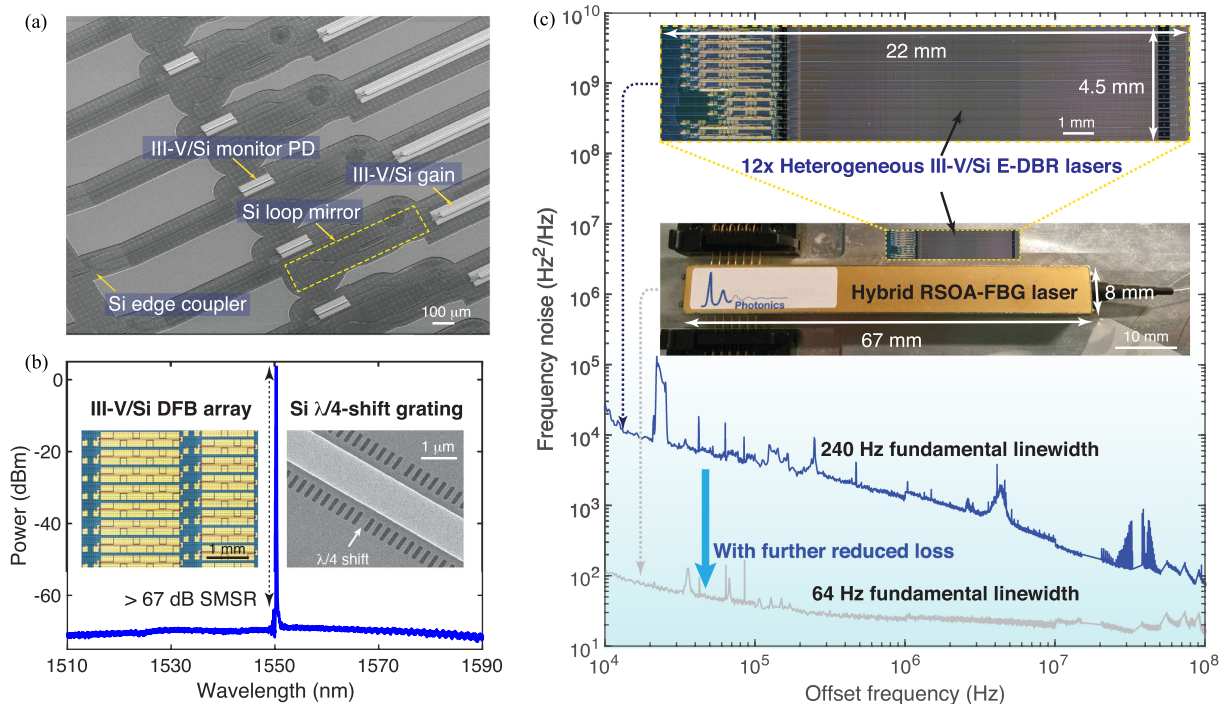
Fig. 3.   (a) SEM image showing the III-V/Si gain section and its transition to passive Si loop mirror-based on-chip reflectors. Image also shows III-V/Si monitor PDs and Si edge-couplers for facet coupling. (b) Optical spectrum of a III-V/Si DFB laser with over 67 dB SMSR. Insets show the DFB array picture and SEM image of a Si $\lambda/4$-shift Bragg grating. (c) Device pictures and frequency noise comparison of heterogeneous III-V/Si E-DBR lasers and a hybrid RSOA-FBG laser [30].

laser Schawlow-Townes linewidth without external feedback, A is the ratio of external passive Si cavity length to the active III-V/Si gain section length, and B includes the detuned loading effect [32].

The maximum output power of this laser is over 30 mW in the Si waveguide and the fundamental linewidth is down to 240 Hz. The fundamental linewidth value is derived from the white-noise-limited frequency noise floor of the frequency noise spectrum. Fig. 3(c) shows its frequency noise spectrum comparison with a commercially-available hybrid integrated RSOA-FBG (reflective semiconductor optical amplifier-fiber Bragg grating) laser [30]. The heterogeneously integrated E-DBR laser frequency noise performance is approaching that of the hybrid-integrated RSOA-FBG laser, while it holds advantages on the device scalability and lithographically-defined grating uniformity. With further reduced waveguide loss, the frequency noise performance should be comparable with the much larger RSOA-FBG laser. These high-power, low-noise lasers are suitable for applications including coherent optical communications, microwave photonics and LiDAR.

2) Ring-Resonator-Based Tunable III-V/Si Lasers: Wavelength-tunable lasers add additional flexibility in these applications, and find further utilization in wavelength division multiplexed (WDM) communications and sensing systems, such as spectroscopy and optical frequency domain reflectometry (OFDR) [33]. Heterogeneous silicon photonic integration not only allows for lithographic alignment and manufacturing scalability, but also capitalizes on silicon waveguides as a superior low-loss platform over monolithic III-V-based

photonic platforms. These low loss waveguides catalyze a new suite of functionalities, resulting in tunability up to 118 nm and instantaneous linewidths below 100 Hz [34].

By incorporating thermally-sensitive silicon waveguides in the laser cavity, heterogeneous integration allows for widely tunable lasers while maintaining low round-trip losses. Resistive heaters can be placed in close proximity to the silicon waveguides to provide a thermally induced change in refractive index, thus changing the cavity length and lasing wavelength. The cladding thickness between the metal heaters and silicon waveguide offers a trade-off between tuning efficiency and absorptive losses [35]. One way of achieving wide tunability is by integrating thermally tunable ring resonators into the laser cavity. One or more ring resonators can be incorporated in a Sagnac reflector to form a laser mirror. Connecting two or more ring resonators with bus waveguides on the drop ports creates a wider effective free spectral range (FSR) due to the Vernier effect, resulting in a broader tuning range than that of a single ring resonator. These results have been reviewed in [24]–[33], [36].

An alternate strategy mimicking external cavity lasers employs multiple ultra-low-loss, large radii ring resonators to enable even wider tunability and further reduced instantaneous linewidth [24]–[37], [38]. These high-Q ring resonators are facilitated by ultra-shallow-etch (56 nm) silicon waveguides, allowing for the optical mode to be weakly guided [27]. This has two major benefits. First, the modal overlap with the waveguide sidewalls is reduced, which mitigates sidewall roughness induced scattering. Second, the cross-sectional modal area is expanded, which distributes the optical power, mitigating
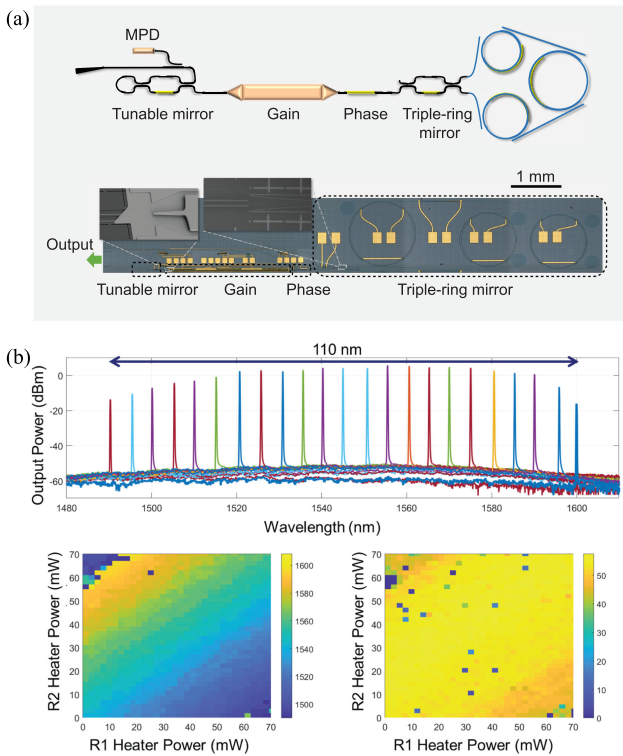
Fig. 4. (a) Device schematic design (top) and picture (bottom) of an 3-ring-based III-V/Si widely tunable laser. (b) Stacked optical spectra of the 3-ring-based III-V/Si widely tunable laser operating at different wavelengths (top). Bottom plots show the wavelength tuning map and associated laser SMSR map corresponding to different heater power values applied on the two Vernier rings [36].

the effects of intensity-dependent nonlinear loss, particularly two-photon absorption (TPA) and TPA-induced free carrier absorption (FCA) [39]. The cost of the ultra-shallow etch and weak guiding is bending loss, therefore larger bending radii are necessary. Due to the smaller FSRs of these larger rings, more than two rings are necessary to suppress close-in side modes and facilitate single mode operation. The ring dimensions and coupling coefficients are thus tailored to balance wide tunability with mode selectivity.

Fig. 4(a) shows the schematic design diagram and an image of a device with three ultra-shallow etch, large-radii ring resonators forming the back mirror in the laser cavity. This design is supplemented by MZI-based thermally tunable couplers, allowing the coupling ratio and thus the reflectivity to be adjusted across the wavelength tuning range. These tunable reflectors can be optimized to tap more power from the front mirror or ASE-filtered light from the ring resonator mirror. A stitched microscope image of a widely-tunable III-V/Si laser shown in also Fig. 4(a), featuring a III-V/Si gain section, Si MZI-based tunable coupler, Si triple-ring mirror and phase tuner.

Fig. 4(b) displays the wide tuning range of these devices, from 1490 nm to 1600 nm, with each spectrum exhibiting over 45 dB SMSR over the entire tuning range. These lasing spectra were taken by systematically stepping the heater powers in each of the rings across the full Vernier FSR of 110 nm, while also optimizing the phase section power to maximize output power. This effective FSR is wide enough that the InAlGaAs multiple

quantum well (MQW) gain bandwidth becomes the limiting factor for laser oscillation, as evidenced by the drop in power at the edges of the tuning range.

This passive cavity architecture not only features tunable, narrowband filtering, but also enables significant reduction in the quantum-limited white frequency noise. This is due to the resonantly enhanced fraction of the cavity contributing to filtering (i.e. the optical mode in the ring resonators) vs. the portion contributing to phase noise (i.e. the gain section generating ASE). The linewidth narrowing effects of this process are quantified by the 'A' parameter in the modified Schawlow-Townes linewidth equation, as discussed before [24], [36]. The Schawlow-Townes (also instantaneous, fundamental, intrinsic, or quantum-limited) linewidth can be further narrowed by detuning the lasing frequency to the red side of the dispersive mirror, taking advantage of an optical negative feedback loop. This detuned loading effect (the 'B' factor), relies on the coupling between phase and amplitude unique to semiconductor lasers, which is described by α_H, the linewidth enhancement factor [40].

3) Heterogeneous Integrated III-V/Si/Si$_3$N$_4$ Lasers: As discussed in the previous section, Si$_3$N$_4$ waveguide loss can be orders of magnitude lower than that of Si. Further noise reduction through laser active-passive integration can be achieved if Si$_3$N$_4$ can be integrated within the laser cavity. There has been extensive research into hybrid integrated lasers with single-wavelength or ring-based wavelength-tunable Si$_3$N$_4$ cavity [32], [41]–[44]. Heterogeneous integration of a silicon nitride cavity eliminates the time-consuming process of coupling and packaging the laser gain chip and Si$_3$N$_4$ chip, and increases the device robustness. Additionally, it enables wafer-scale production of lasers with integrated Si$_3$N$_4$ cavities.

Due to the requirement of high temperature processing for low-loss Si$_3$N$_4$ films, heterogeneous integration with Si$_3$N$_4$ usually requires the low-loss Si$_3$N$_4$ to be processed at the front-end, followed by wafer bonding process which limits the overall temperature budget of the remaining process. Another issue with a direct III-V/Si$_3$N$_4$ heterogeneous structure is the index mismatch between the normal III-V epi stack ($\sim$2 μm thick) with Si$_3$N$_4$ waveguide preventing efficient evanescent mode coupling and transitions in between. A multilayer III-V/Si/Si$_3$N$_4$ structure is employed to bridge the index mismatch using an intermediate Si layer [8]. Fig. 5(a) shows the integration approach that includes multiple wafer bonding and oxide deposition steps for the multilayer structure.

The III-V/Si/Si$_3$N$_4$ laser leverages the Si$_3$N$_4$ spiral shaped Bragg grating as the external cavity (Fig. 5(b)). The grating length is 20 mm, packed in a footprint of only 3.5 mm $\times$ 3.6 mm due to the spiral shape. It provides single-wavelength feedback around 1548 nm. In order to achieve high coupling efficiency between the InP layer and Si$_3$N$_4$ layer, an InP-Si taper and Si-Si$_3$N$_4$ dual-level taper are used to evanescently transiting the corresponding optical modes [8].

Lasing from the Si$_3$N$_4$ cavity is verified using the infrared camera image captured during measurement (Fig. 5(b) inset). The laser multilayer cross sections including InP/Si gain and Si/Si$_3$N$_4$ are shown in Fig. 5(c). The laser wavelength follows the grating response and is stable in terms of temperature change
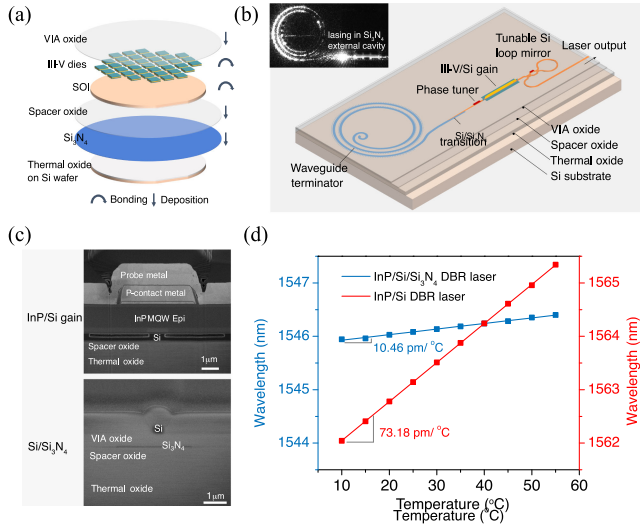
Fig. 5. (a) Schematic of the multilayer heterogeneous integration process. (b) Device design illustration of a III-V/Si/Si_3N_4 laser with Si_3N_4-based spiral grating. The inset IR images shows lasing within the Si_3N_4 cavity. (c) Cross-sectional SEM images showing the InP/Si gain and Si/Si_3N_4 section. (d) A comparison of temperature-dependent wavelength shift of the III-V/Si/Si_3N_4 laser and III-V/Si E-DBR laser [8].

due to the low thermo-optic coefficient of Si_3N_4 and SiO_2. The wavelength drift dependence on temperature is 10.46 pm/^{o}C, which is 7x smaller than that of an InP/Si E-DBR lasers with similar cavity length (Fig. 5(d)). We anticipate that these lasers, together with Si_3N_4 based arrayed waveguide gratings (AWGs) could enable DWDM (dense wavelength division multiplexing) applications instead of CWDM (coarse wavelength division multiplexing) in datacenter interconnects as the lasing wavelengths are much more stable against temperature drift, which minimizes the inter-channel crosstalk. The output power and laser linewidth of the first-generation of these lasers are still limited by the Si_3N_4 waveguide loss. A new generation of III-V/Si/Si_3N_4 E-DBR lasers have over 20 mW output powers with Lorentzian linewidth down to 400 Hz [45]. Another approach to achieve such a multilayer structure is to use an α-Si layer for the immediate index bridging. Heterogeneously integrated SOAs and lasers on SiN are thus demonstrated using micro-transfer printing techniques [46].

4) Heterogeneous Integrated QD/Si Lasers: QD lasers offer new opportunities for improved performance towards lower threshold current density, narrower linewidth, higher temperature stability, better immunity to epitaxy and fabrication defects, and reduced linewidth enhancement factor (α_H) [5]. These features make QD lasers particularly attractive in data communication applications, where laser drive current and thermoelectric cooling can make a substantial impact on the overall energy efficiency. On the other hand, reflection insensitivity in single-wavelength QD lasers can significantly reduce packaging complexities and enhance integration density associated with isolator integration. These favorable material merits make it ideal to serve as the optical gain medium on silicon in both heterogeneous and monolithic fashions. For heterogeneous QD lasers in O-band, similar wafer bonding and device process are implemented and GaAs-based QD epitaxial material can
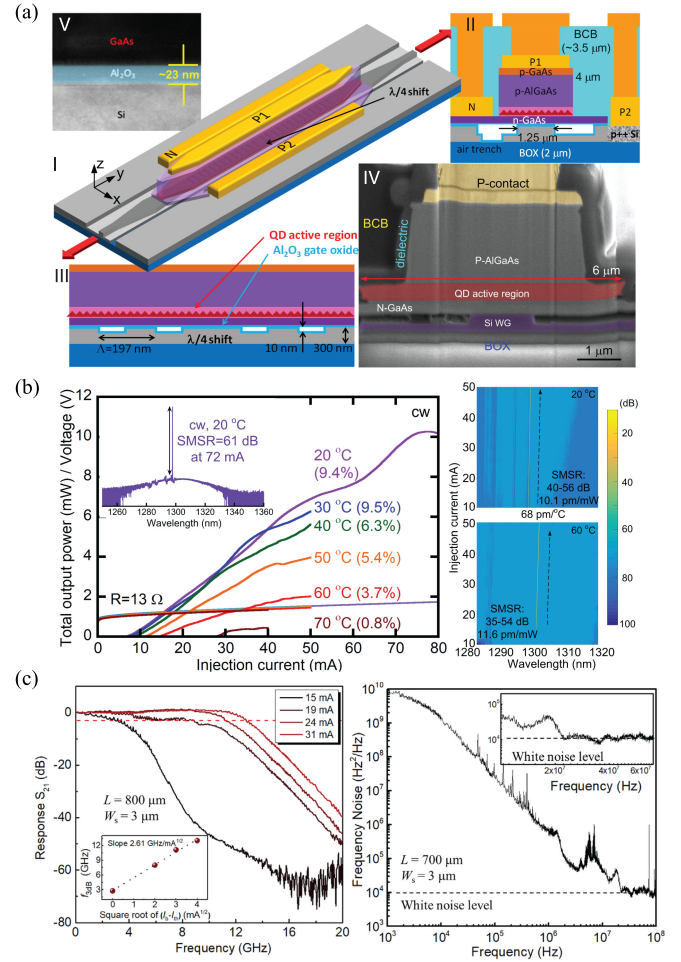

Fig. 6. (a) Device schematic of a GaAs/Si QD DFB laser in different configurations (I-III) and device cross-sectional SEM image and transmission electron microscopy image of the MOS (metal oxide semiconductor) capacitor, MOSCAP (IV-V). (b) Temperature-dependent light-current-voltage characteristic of the GaAs/Si QD DFB laser shown in a, and its spectral map up to 50 mA injection current at 20°C and 60°C, respectively [50]. (c) Small-signal modulation responses (left) and frequency noise spectrum (right) of a high-speed GaAs/Si QD DFB laser [51].

easily replace InP-based QW epitaxial material to build different device designs. The first demonstration of light coupling between QD lasers and Si waveguides was achieved by B. Jang *et al.* [47] and G. Kurczveil *et al.* [48]. Since then, various types of heterogeneously integrated QD lasers have been demonstrated including DFB lasers [49]–[51], colliding pulse modelocked lasers [52], microring lasers [53], and tunable lasers [54]. Since the light is evanescently coupled between the QD active region and the low-loss Si waveguides, the laser cavity design and the gain active region can be separately optimized (Fig. 6(a)). The GaAs-based QD epitaxial structure typically has five to eight stacked QD layers. Due to the enhanced carrier localization in QDs, the non-radiative recombination impact to the laser operation and reliability at the etch-exposed QD active region are greatly reduced. This makes it feasible to realize mesa widths on the order of 2 μm without imposing an obvious penalty on the lasing threshold. The narrow mesa width laterally confines both the current channel and the optical mode, efficiently suppressing high order modes as well as avoiding current spreading issues

that are beneficial for higher laser efficiencies. Therefore, proton implantation to define the current channel is not necessary.

By engineering the QD epi stack and Si grating designs, largely improved performance is shown in heterogeneously integrated QD DFB lasers (Figs. 6(b) and (c)): up to 100 ^oC lasing in CW mode [49], a demonstrated CW threshold current density as low as 134 A/cm^2, up to 9.5% wall plug efficiency, and a single-wavelength operation with SMSR up to 61 dB in broad spectral and injection current ranges based on a shallow etched first-order grating [50], an SMSR of 60 dB and a Lorentzian linewidth of 26 kHz based on a first order side-hole gratings [51]. This Lorentzian linewidth of tens of kHz is two orders of magnitude lower compared to that of the typical solitary QW laser linewidth of several megahertz, attributed to the much lower α_H of QDs and lower loss of Si waveguide. In the latest design, DFB gratings are formed by patterning a surface corrugation on top of the Si waveguides, and the widths are tailored to accommodate a suitable κ, low radiation loss, and reliable fabrication process.

The QD/Si heterogeneous DFB lasers find applications in data interconnects when combined with suitable modulation methods. Direct modulation of QD lasers are usually limited by the finite intraband relaxation time and gain saturation effect. However, the latest results (Fig. 6(c)) show 3-dB modulation bandwidth ($f_{3\,dB}$) of 13 GHz attained from a directly-modulated QD/Si heterogeneous DFB laser [51]. The results can be further improved by applying bandwidth enhancement techniques including adding appropriate facet coatings, depositing the metals on lower-capacitance dielectrics and so on. Another approach is to utilize external modulation for the QD/Si heterogeneous DFB laser [50]. 25 Gb/s data-links isolator-free modulation with a metal-oxide semiconductor capacitor microring modulator has been achieved. Their narrow linewidth characteristic makes them attractive for coherent communications as well.

As previously discussed, heterogeneous integration allows gain material to be combined with high-performance passive silicon circuits, enabling widely tunable and narrow linewidth lasers. In the same way, QD gain material can be integrated together with low-loss silicon waveguides to form a laser cavity, but with the added advantages of QD over QW lasers. Tunable lasers with QDs as the gain material have been implemented together with Si ring-resonator-based external cavities [54]. For a laser based on an MZI and 2-ring mirror, the demonstrated tuning range is 52 nm in the O-band with at least 45 dB SMSR and Lorentzian linewidth below 10 kHz.

C. Comb Lasers

Comb lasers are ideal for multi-wavelength data interconnects due to the natural fit with WDM systems. Contrary to single-wavelength laser arrays that are deployed in conventional long-haul WDM systems, comb lasers provide a solution that dramatically increases the number of multiplexed signal channels without the need to rely on multiple laser sources. Since the intrinsic energy consumed by a laser to reach threshold does not scale with the number of channels for comb lasers, the approach of using one laser instead of multiple lasers for multiple channels is critically important to lower the overall power consumption.

Two types of comb lasers are now being deployed into system demonstrations, including mode-locked lasers and nonlinear Kerr frequency combs. In both scenarios, integrated photonics plays an important role. There has been dramatic progress in the past decade developing integrated semiconductor mode-locked lasers on silicon [57], [58] and nonlinear Kerr frequency comb generation on various platforms built on silicon substrates [59]–[66].

Heterogeneously integrated mode-locked lasers on silicon serve as multi-wavelength sources capable of integration with other devices in silicon photonic circuits. Recent developments of heterogeneous laser integration with Kerr optical frequency combs brings low-noise comb sources one step closer to advanced chip-scale deployment with mature silicon photonic functional devices [29].

1) InP/Si QW Mode-Locked Lasers: Heterogeneously integrated III-V/Si mode-locked lasers using integrated mirrors do not rely on cleaved or polished facets for laser feedback, and hence the mode spacing can be controlled quite accurately, such that with slight tuning of the gain current, a desired spacing can be achieved with high yield [67]. Saturable absorbers can be implemented directly using the laser gain material by reverse biasing.

Fig. 7(a) shows a schematic illustration of a III-V/Si colliding pulse mode-locked laser [55]. The on-chip reflector is based on a Si loop mirror. For better performance, the loop mirror is designed to be spline shaped reflector to minimize the overall loss [58]. A saturable absorber is placed at the middle of the structure. To reduce back-reflection from the uncoated Si facet, the output waveguide is tilted at 7 degrees. Mode locking is achieved with certain bias current and reverse bias on the saturable absorber. Wide mode locking range is obtained with gain currents ranging from 60 to 200 mA and SA reverse bias from 2.5 V to 5 V. Stable mode locking is verified by the RF beating tone, which has over 60 dB signal-to-noise ratio. The minimum pulse width is 1.08 ps with passive mode locking and is further reduced to 890 fs by hybrid mode locking using an external RF source. An additional advantage of heterogeneous mode-locked lasers is the low-loss Si waveguides or SiN, which can be utilized for higher performance, including dispersion compensation, phase noise reduction and so on [68], [69]. Recent demonstrations include record-low repetition rate mode-locked-lasers with 1-GHz and 755-MHz mode spacing, using low loss Si and SiN waveguides respectively [70], [71].

2) GaAs/Si QD Comb Lasers: Quantum dot material features an inhomogeneously broadened gain spectrum and ultrafast carrier dynamics, which are ideal for comb laser operation [5], [72]. QD-based III-V/Si comb lasers have demonstrated remarkably flat optical spectra, which distinguish them from traditional mode-locked lasers, as shown in Fig. 7(b) (left) [56]. The device consists of a 1.2-mm-long gain section, and a 120-μm-long saturable absorber which are centered between the mirrors. The front and back mirrors are formed by multimode interferometers and loop mirrors having reflectivities of 50% and 100% respectively. An external cavity was formed between the front mirror and the grating-based output coupler, which resulted in a channel spacing of 101 GHz. While the device contained a saturable
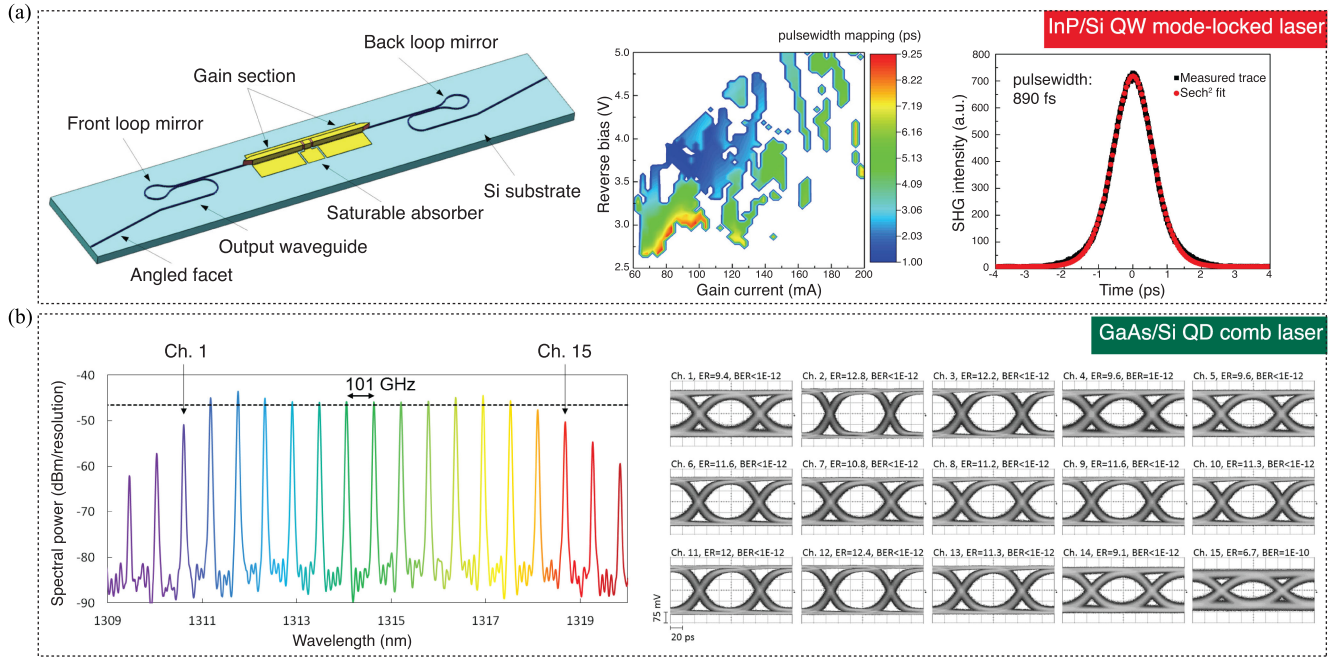
Fig. 7. (a) Schematic of an InP/Si QW mode-locked laser (left), pulse width mapping as a function of the gain section forward bias current and SA section reverse voltage under passive mode locking state (middle) and single pulse autocorrelation trace with sech^2 fit (right) [55]. (b) Optical spectrum of QD-based III-V/Si comb laser (left). The flat spectrum reduces the need for channel equalization at the receiver; Eye diagram and BER of each channel from the device in a after external modulation at 10 Gb/s (right) [56].

absorber, the optical output is CW (continuous wave, no pulses are observed), which reduces unwanted nonlinearities in the link and potentially increases the device reliability. Filtering out one comb line at a time and modulating it externally yields eye diagrams and bit-error-rate (BER) values shown in Fig. 7(b) (right). We note open eye diagrams and BER values or 10^{-12} or lower in 14 of the 15 channels. The width of the comb can likely be broadened by tuning the total cavity dispersion (by using an appropriately chirped grating for example) and spatial hole burning (by offsetting the gain section from the cavity center [73]).

3) Laser Soliton Microcombs: Optical frequency combs generated in on-chip microresonators, termed as 'microcombs' have been extensively studied and deployed in many applications in the past decade [23], [26], [74]. Emerging platforms for microcomb generation are mostly built on silicon substrates. This is largely due to the requirement for compact and tight mode confinement for microcomb generation and the benefits of high index contrast from Si-based platforms.

Integrated photonics enables miniaturization of frequency comb generation on a chip scale. However, in most applications lasers and amplifiers are still based on bulky and expensive table-top equipment. Semiconductor lasers are normally too noisy for soliton generation. Recent development of integrated laser-comb systems utilizing self-injection locking eliminates the need for an optical isolator as well as a narrow-linewidth pump laser, since the laser-resonator system itself relies on the resonator feedback signal to simultaneously reduce the laser linewidth and generate optical frequency combs [75], [76].

Heterogeneous integration allows this laser-resonator to be integrated on a monolithic substrate to enable high-performance multi-wavelength laser sources directly on chip. III-V materials

and low-loss nonlinear materials are combined through wafer bonding. The first demonstration of such devices is illustrated in Fig. 8(a). A high-power InP/Si DFB single-wavelength laser outputs the pump light with λ around 1550 nm, entering the non-linear microresonator for comb generation. The back-scattered signal from the high-Q Si$_3$N$_4$ microresonator is fed back to the laser. When the relative phase between the forward and backward signal is matched, the resonant feedback pulls the laser frequency into the resonator mode, injection locking the laser. Different frequency comb states are generated depending on the laser frequency detuning with respect to the Si$_3$N$_4$ microresonator resonance. The wafer picture and multiple dies of devices are shown in Fig. 8(b).

The entire device with multilayer structures is heterogeneously integrated on a silicon substrate with wafer-scale processing. Similar to the III-V/Si/Si$_3$N$_4$ lasers discussed in the previous section, silicon is used as the index matching layer between the III-V gain and ultra-low loss Si$_3$N$_4$. Similarly, a thermo-optic resistive heater on the Si waveguide is used to tune the phase between the laser and nonlinear resonator, thus allowing electrical control of comb state generation.

The fabrication process of the laser soliton microcomb devices is based on multilayer heterogeneous integration, compromising two wafer bonding steps and several planarization steps [29]. The device can output a single soliton state with 100-GHz repetition rate (Fig. 8(c)) and soliton crystal states with larger comb spacing. Due to the laser self-injection locking to the high-Q microresonator, the DFB laser frequency noise is reduced by 10 to 30 dB depending on the offset frequency range. The Lorentzian linewidth is 25 Hz for the self-injection locked pump line in the single-soliton state and the low frequency noise is also transferred to the other comb lines. Further laser linewidth
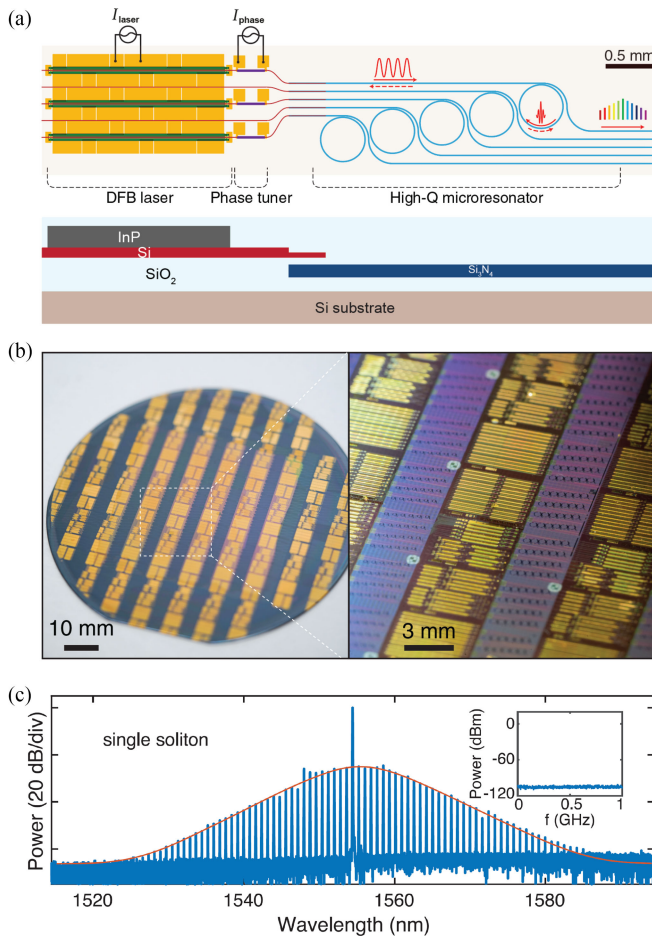
Fig. 8. (a) Device schematic and (b) images of laser soliton microcomb devices based on InP/Si/Si_3N_4 multilayer structure. (c) Optical spectrum of the generated 100 GHz-repetition rate single soliton state [29].

Fig. 9. (a) Configuration of a III-V/Si OPA system with a $1 \times N$ star coupler, III-V/Si phase shifter array with a pitch of 4 μm, and grating emitter array. Right panel: schematic cross-section of the III-V/Si phase shifter array with locally opened n/p contact for probing one shifter on top. (b) Images of a fully fabricated 240-channel (upper panel) and 32-channel (lower panel) OPAs with enlarged SEM images for different parts of the OPA. (c) Measured beam profiles at 1550 nm wavelength with the beam steering across the field of view in the Ψ-axis at a 2.8° increment in the 32-channel OPA. The right inset shows the IR images of the main beam when steered by phase in Ψ-axis. (d) Measured beam profiles along θ axis ($\Psi = 0$) with the beam steering when tuning the wavelength from 1450 nm to 1650 nm at a 10 nm increment. The top inset shows the IR images of the main beam when tuning wavelength in θ-axis [77].

reduction can be achieved with resonators of higher Q and larger mode volume.

The demonstration of heterogeneously integrated soliton microcombs provides another solution for on-chip multi-wavelength sources with low noise performance that is unattainable from semiconductor mode-locked lasers. Heterogeneous integration of gain materials with ultra-low loss photonic circuits is the key and can be expanded to many other material platforms that have unique properties. For example, III-V integrated with $LiNbO_3$ which has a strong electro-optic effect and second order nonlinearity can offer the generation and modulation of the soliton microcomb signals, fully-integrated E-O combs, second/third-harmonic-generated light or ultra-high-capacity optical transceivers.

III. SILICON PHOTONIC INTEGRATED CIRCUITS

In additional to individual devices, heterogeneous integration also shows advantages in a series of photonic integrated circuits and this section will cover some of the most recent results.
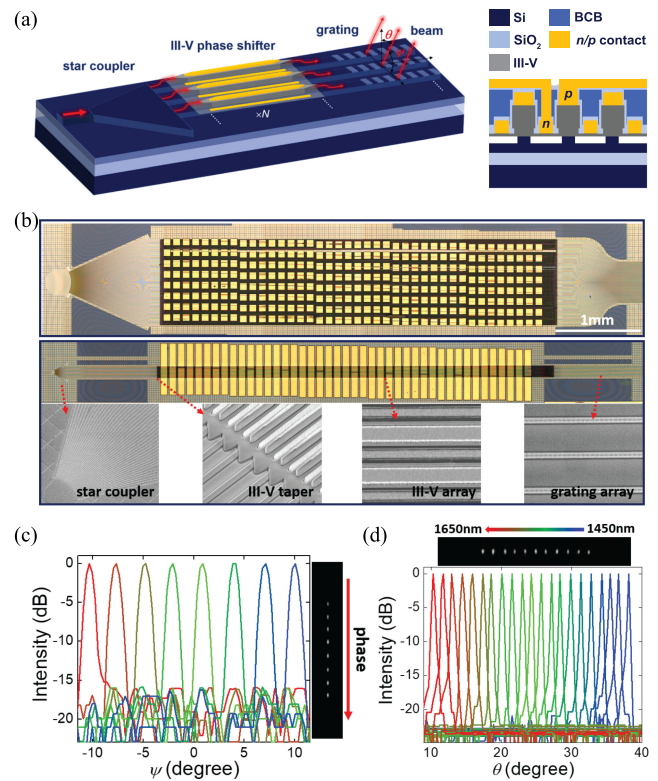
A. Optical Phased Arrays

Heterogeneous III-V/Si devices can be regarded more than as just stand-alone function units which are usually spaced at more than 100 μm. Heterogeneous silicon photonic PICs see tremendous progress in both the device scale and device performance. Recently, Si photonics has attracted tremendous attention in chip-based fully solid-state LiDAR applications, e.g. optical phased arrays (OPAs). III-V/Si heterogeneous integration can offer high-performance active building blocks like high-efficiency phase shifters with low power consumption in addition to laser sources, providing a promising solution for complete on-chip LiDAR systems. On the other hand, PICs for LiDAR (e.g. OPA-based system) involves thousands of components in a limited reticle area and thus requires large-scale and dense integration.

To make use of efficient electro-optic properties in III-V, heterogeneous integration technology has been further extended for high-density integrated III-V/Si PICs at large scales. Fig. 9(a) shows an OPA design with a III-V/Si phase shifter array with
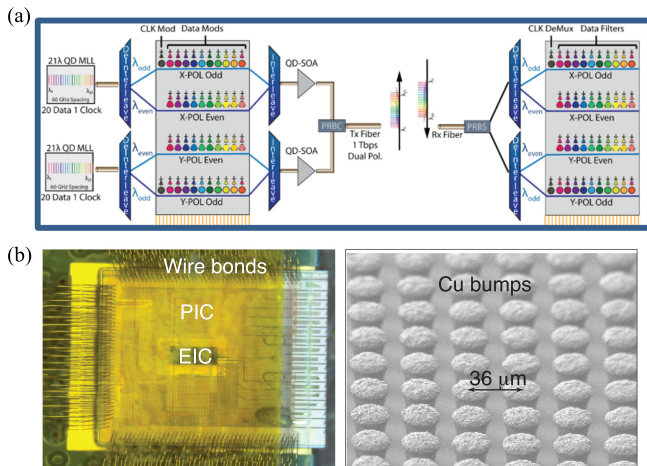
(a)

(b)

Fig. 10. (a) Architecture of a low power consumption transceiver using QD-MLL sources and integrated linear ring modulator arrays for an 1-Tb/s link. (b) Image showing the 3D flip-chip bonded EIC and PIC (left). The SEM image on the right shows the densely-spaced copper pillar bumps for the 3D EIC-PIC integration [67].

a pitch of only 4 μm. The cross-section view shows the density of the array. Fig. 9(b) shows the fabricated 240-channel and 32-channel OPAs. The number (N) of phase shifters are scalable in practice. These phase shifters exhibit low residual amplitude modulation ($\sim$0.15 dB in C-band), low static power consumption (a few nW), low operating voltage (about -1 V in C-band), wide optical bandwidth (200+ nm) and high operating speed ($>$1 GHz), suitable for OPA applications. Notably, they exhibited uniform performance, proving the reliability of the heterogeneous III-V/Si platform for larger-scale integration. In a tested 32-channel OPA, 2D steerable far-field beams with a beam width of $0.78° \times 0.02°$ and a field of view of $22° \times 28°$ were demonstrated through both phase (Ψ-axis) and wavelength tuning (θ-axis with wavelength from 1450 nm to 1650 nm), respectively, as shown in Fig. 9(c). The beam divergence can be further improved by scaling up the element number of OPA and optimizing the optical antenna design. Combined with previously realized III-V/Si high-power lasers, amplifiers, and detectors on the same heterogeneous integration platform, high-power and high-quality steerable beams out of a single chip become achievable. Related systems for applications such as monolithic chip-fashioned LiDAR can be thus realized.

B. Integrating Silicon PIC and EIC

Silicon photonics allows for high-confinement, low-footprint devices. Ring modulators and demultiplexers with as-fabricated resonant offsets and driver electronics flipped on top are a compact, energy-efficient means of achieving high capacity communication links ($>$1 Tb/s). The comb sources discussed above are ideal to be integrated with linear arrays of rings to achieve an ultra-dense, high-capacity WDM link with sub-pJ/bit power consumption [72]. Fig. 10(a) shows a 1 Tbps transmitter utilizing 20 wavelengths at 25 Gbps [67]. Fig. 10(b) shows a picture of 3-D packaged PIC and EIC (electronic integrated circuit) with copper pillar bumps to minimize the electrical link

length and associated high device capacitance. The copper pillar bumps are closely spaced with 36 um pitch to achieve high bandwidth density ($>$ 1 Tb/s/mm^2). Wire bonds to ring tuning electronics are used as shown in Fig. 10(b) and could be replaced by embedded PIC and control electronics in a silicon interposer to further lower the electrical power consumption.

Heterogeneous photonic integration refers to wafer bonding technology that integrates multiple photonic material groups on silicon, analogy to how electronics illustrates the capability to integrate separately manufactured components into a higher level assembly (System-in-Package, SiP). Heterogeneous integrated silicon photonic chiplets, with its CMOS-compatible nature, are ideal for dense electronic-photonic integration to solve the electronic and energy consumption bottleneck problems of electrical ICs [19].

IV. COMMERCIALIZING HETEROGENEOUS SILICON PHOTONICS

Heterogeneous integration of the semiconductor lasers with silicon optical modulators to form highly functional transmitter PICs has tremendous benefits in terms of lower cost, lower packaging complexity, and high-volume scalability. When compared to alternative techniques such as butt-coupling of lasers directly to silicon PICs, or using fiber to bridge the two chips together, heterogeneous integration allows for the entire transceiver to be fabricated and tested at a 300 mm wafer level [16]. In addition to these economic and scaling benefits, integration of the laser and modulator also has multiple performance benefits stemming from the higher level of integration. Removing a fiber-to-chip optical coupler between the laser and modulator leads to less overall loss, which can improve the link budget. The emitted light from a semiconductor laser is also highly polarized, eliminating any polarization-based ambiguity at the input to the modulator. Intel has demonstrated the success of large-scale, high-volume heterogeneous silicon photonics through its silicon photonics platform and products, which are shipping millions of units per year [16], [19], [78].

Looking forward, as bandwidth requirements continue to increase beyond 400 G and 800 G due to the explosion in data center traffic, the size and power consumption of PICs need to decrease, analogous to Moore's Law. One such approach is to utilize microring modulators (MRMs), which are hundreds of times smaller than conventional Mach-Zehnder modulators. In addition to the footprint reduction, MRMs also have higher modulation efficiency, lower power consumption, and can be engineered to have large electro-optic (EO) bandwidth. Intel's previous work on MRMs showed EO bandwidths of more than 50 GHz and PAM4 eyes at 128 Gbps [79]. More recently, optimizations to the p-n junction design have allowed for the data rate to be increased to 192 Gbps PAM4 and 128 Gbps NRZ [80], making the MRM device suitable for 800 Gb/s optical interconnects and beyond.

Due to the resonant nature of MRMs, they require active control of the resonance condition to compensate for changes in the ambient temperature. This is typically done through integrated doped silicon or metal heaters placed near the MRM to align it to the laser wavelength. When the laser is integrated
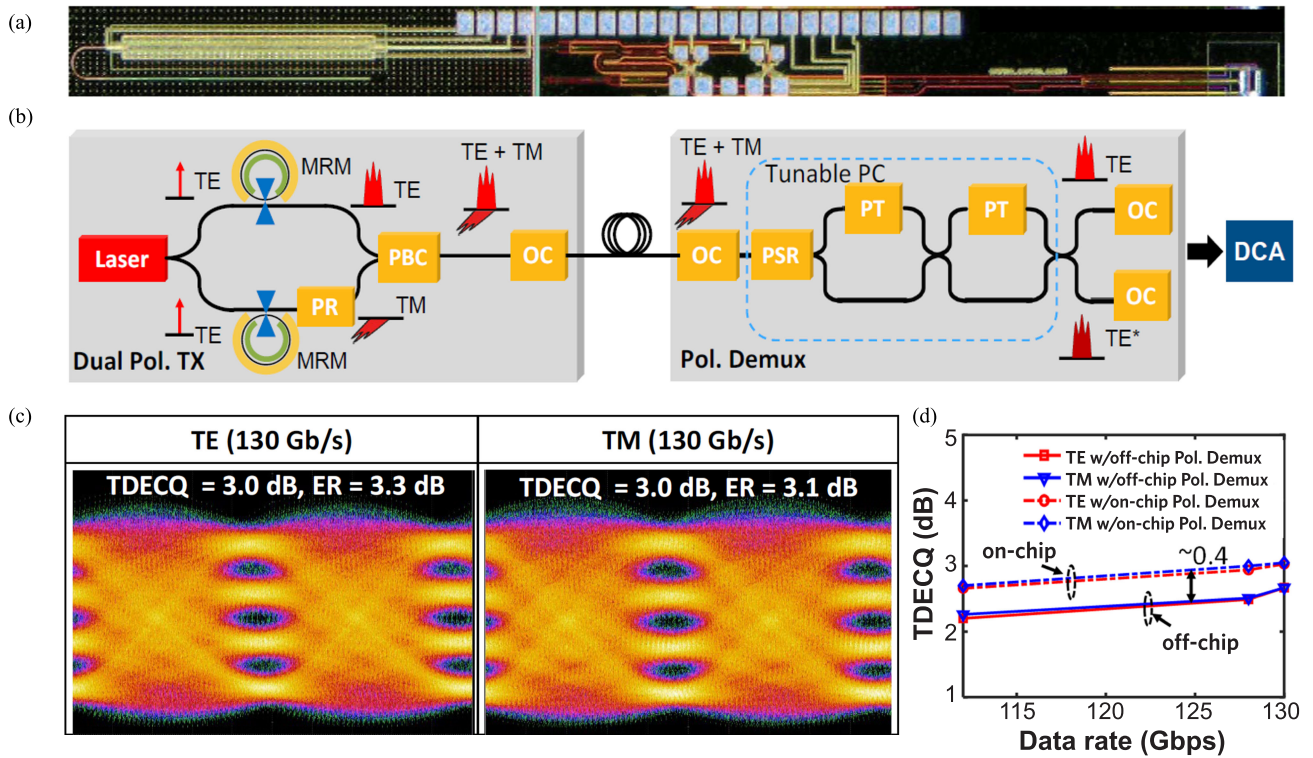
Fig. 11. (a) Micrograph and (b) schematic of a dual-polarization transmitter with integrated laser, MRM, polarization rotator (PR), polarization beam combiner (PBC) and optical coupler (OC). The polarization demux chip consists of a polarization splitter, a rotator (PSR), and several phase tuners (PT). (c) The received 2×130 Gbps PAM4 eyes are measured on the DCA, with a TDECQ of 3.0 dB. (d) A comparison is made between the integrated polarization demux chip and off-chip fiber polarization components.

with the MRM on the same chip, the walk-off between the MRM resonance and laser wavelength due to temperature change is reduced when compared to the case where the laser is on a separate chip at a fixed temperature. This is another benefit of heterogeneous integration, and a fully integrated transmitter with laser, MRM, co-packaged CMOS driver and thermal control is shown in [81]. The scalability of heterogeneously integrated lasers with MRMs in Intel's silicon photonic platform is shown, in which 800 gigabits per second are transmitted across 8 parallel optical channels, each operating at 106.25 Gbps PAM4 [82]. Eight transmitters with integrated laser, MRMs, and thermal control are simultaneously operational and characterized. The full PIC and package have a total of 16 optical channels, with a full capability of 1.6 Tbps, while maintaining a smaller footprint than a 100 G pluggable QSFP28 module.

As discussed in the previous section, WDM is an effective technique to further scale the bandwidth, especially on a per fiber basis. MRMs are perfect candidates for WDM, as the ring modulators can be easily cascaded along a single waveguide to increase the total bandwidth per fiber/waveguide. A recent example is provided in [83], in which error-free transmission is demonstrated in a PIC with 4 WDM channels with accompanying CMOS IC at 50 Gbps per channel. Other recent examples with varying levels of integration are presented in [84], [85]. In such dense WDM systems, the wavelength spacing of the lasers and the MRMs need to be tightly controlled. For heterogeneously integrated lasers on silicon, the laser wavelength can be defined by gratings patterned on the silicon. The superior lithography and tight process control in a 300 mm CMOS fab is

critical to achieve this task. Across an entire 300 mm wafer, the wavelength of the laser is controlled with a standard deviation of 0.2 nm [86]. Considering that lasers are in proximity to each other, such as those within a single PIC, the wavelength control can be even tighter. This allows for the lasers and rings in a WDM transmitter to be nearly aligned to a predetermined wavelength grid as fabricated. Some further fine-tuning of the wavelength may still be required and can be accounted for using promising techniques such as germanium trimming of ring resonators post-fabrication [87], which was demonstrated to permanently align all the ring resonators across a 300 mm wafer within 32 pm of a target wavelength.

Yet another vector to scale bandwidth is to utilize polarization division multiplexing (PDM), in which data is further encoded in the transverse electric (TE) or transverse magnetic (TM) polarization of light, effectively doubling the data rate of a transmitter when implemented. This approach is widely used in long-haul coherent links, but not as much within short reach data centers links. A fully integrated dual-polarization heterogeneous silicon transmitter is shown in Fig. 11 [88]. Here, power from a single DFB laser is split between two independent MRMs operating at 130 Gbps each, and then combined into orthogonal polarizations using a polarization rotator and combiner to achieve a total of 260 Gbps data rate for a single wavelength. Since the laser is integrated, there is no need for active polarization control or polarization maintaining fiber for the transmitter. The data is transmitted across a short length ($\sim$3 m) of single-mode fiber, and then de-multiplexed on a separate chip using an integrated polarization controller consisting of a polarization splitter
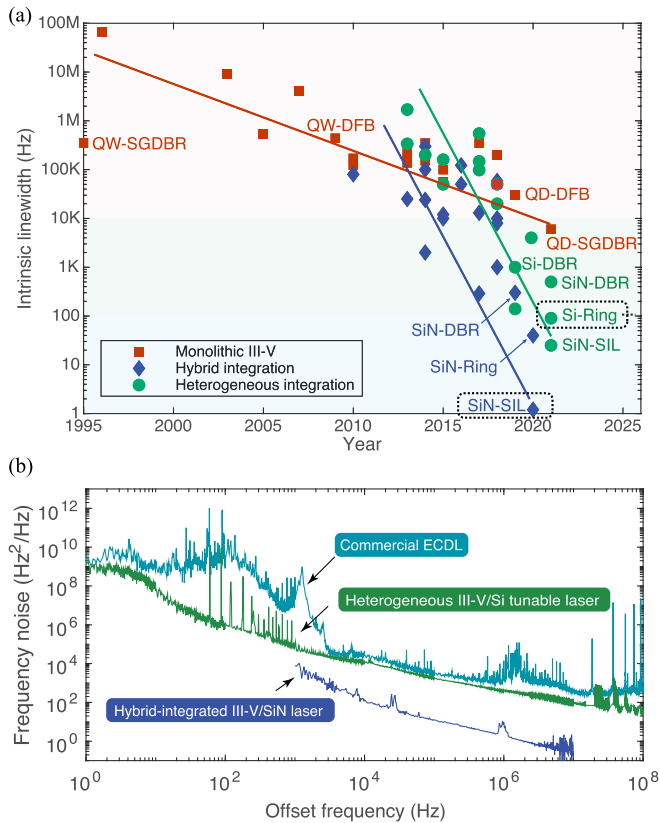
Fig. 12. (a) Semiconductor laser linewidth progression for three different integration approaches [19]. (b) Frequency noise comparison between a commercial ECDL (turquoise), a heterogeneous III-V/Si widely tunable laser (green) and a hybrid-integrated III-V/SiN laser based on SIL (blue). The green and blue curves correspond to the Si-Ring and SiN-SIL data shown in a, respectively [9], [34]. SIL stands for self-injection locking.

rotator, and Mach-Zehnder interferometer [89]. This polarization demux chip compensates for any polarization rotation in the fiber link, and recovers the two initial data streams, which are measured on a digital communication analyzer (DCA) and shown below. For each of the two eyes at 130 Gbps, the transmitter dispersion eye closure (TDECQ) is 3.0 dB, and the difference in TDECQ between an integrated and off-chip polarization demux is only 0.4 dB, showing that the integrated polarization controller is effective for this link over short distances.

V. SUMMARY AND OUTLOOK

We have presented recent progress of heterogeneous silicon photonic devices and integrated circuits. High device performance and high integration level are enabling and extending its applications in the fields of communications, interconnects and sensors. Key metrics of heterogeneous integration are approaching or exceeding monolithic integration or hybrid integration. Heterogeneous integration with optimized actives and passives opens up new opportunities for a whole new class of devices with superior performance to discrete optical components. Narrow-linewidth lasers are a prime example to demonstrate such superiority. Fig. 12(a) summarizes the laser linewidth progress over the past 30 years. For monolithic lasers, the linewidth enhancement factor α_H is the deciding factor and as a result, QD-based lasers can achieve narrower

linewidth than QW-based lasers. Hybrid integration and heterogeneous integration, which utilizes the separately-optimized actives and passives can achieve ultra-narrow linewidth. In this scenario, ultra-low-loss SiN passive waveguides are dominating the best performances. Multiple approaches including extended grating-based external cavities, ring-resonator-based external cavities and self-injection locking with ultra-high-Qs offer different laser operations and contrasting laser linewidth reduction ratios. The design-optimized heterogeneous III-V/Si widely tunable laser linewidth is already performing better than commercial external-cavity diode lasers (ECDLs) using bulky external cavities (Fig. 12(b)). Further laser noise reduction is expected with integrated ultra-high-Q SiN ring resonators, similar to hybrid integration. The heterogeneous integration performance is only 2-3 years behind the state-of-the-art hybrid integration.

While most of the contents covered in this paper is about heterogeneous integration for O-band and C-band applications, it is important to note that heterogeneous integrated silicon photonics is also playing an important role in applications for extended wavelength ranges, including visible, mid-infrared (mid-IR) and so on [90]–[93]. For visible applications, InGaN-based gain materials can be integrated with TiO_2 or SiN waveguides on Si, as the optical refractive index (InGaN and TiO_2) are similar to facilitate efficient evanescent coupling between the active and passive sections [94]. High-Q SiN resonators have been demonstrated in the blue and violet regions [95], and self-injection locked InGaN lasers to these resonators should revolutionize the performance of visible lasers for a variety of display, sensor and optical clock applications. For the mid-IR range, there has been extensive research investigating heterogeneously integrated quantum cascade lasers (QCLs) on silicon [96], interband cascade lasers (ICLs) [97], modulators [98] and photodetectors [99], etc. Other heterogeneous integrated silicon photonics devices that are not discussed in this paper including directly-modulated membrane lasers [100], MOS capacitor-based modulators [101], [102] and avalanche photodiodes [103] are also seeing improved performance. These should help improve optical interconnect link budgets and reduce energy consumption further. Moreover, heterogeneous integration also provides exciting opportunities for novel applications including quantum information processing [104], photonic neural networks [105] and bio-sensing for life sciences [106].

Overall, the commercialization of heterogeneous integrated silicon photonic circuits is evolving rapidly. Close integration with electronics is the key enabler for next-generation high bandwidth datacenter network switches. Reliable, narrow-linewidth and high channel-count heterogeneous laser sources are likely to play a critical role in the next phase, which demonstrates one significant advantage of heterogeneous integrated silicon photonics over other platforms.

REFERENCES

[1] B. E. Saleh and M. C. Teich, *Fundamentals of Photonics*. 2nd ed., Hoboken, NJ, USA: Wiley, 2007.

[2] L. A. Coldren, S. W. Corzine, and M. L. Mashanovitch, *Diode Lasers and Photonic Integrated Circuits*, 2nd ed. Hoboken, NJ, USA: Wiley, 2012.

[3] R. Soref, "The past, present, and future of silicon photonics," *IEEE J. Sel. Topics Quantum Electron.*, vol. 12, no. 6, pp. 1678–1687, Nov./Dec. 2006.

[4] T. Komljenovic et al., "Heterogeneous silicon photonic integrated circuits," *J. Lightw. Technol.*, vol. 34, no. 1, pp. 20–35, 2016.

[5] J. C. Norman, D. Jung, Y. Wan, and J. E. Bowers, "Perspective: The future of quantum dot photonic integrated circuits," *APL Photon.*, vol. 3, no. 3, 2018, Art. no. 0 30901.

[6] M. J. Heck, J. F. Bauters, M. L. Davenport, D. T. Spencer, and J. E. Bowers, "Ultra-low loss waveguide platform and its integration with silicon photonics," *Laser Photon. Rev.*, vol. 8, no. 5, pp. 667–686, 2014.

[7] A. Rahim et al., "Expanding the silicon photonics portfolio with silicon nitride photonic integrated circuits," *J. Lightw. Technol.*, vol. 35, no. 4, pp. 639–649, 2017.

[8] C. Xiang et al., "Narrow-linewidth III-V/Si/Si$_3$N$_4$ laser using multilayer heterogeneous integration," *Optica*, vol. 7, no. 1, pp. 20–21, 2020.

[9] W. Jin et al., "Hertz-linewidth semiconductor lasers using CMOS-ready ultra-high-Q microresonators," *Nature Photon.*, vol. 15, no. 5, pp. 346–353, 2021.

[10] D. Liang and J. E. Bowers, "Recent progress in heterogeneous III-V-on-silicon photonic integration," *Light Adv. Manuf.*, vol. 2, no. 1, pp. 1–25, 2021.

[11] O. Marshall, M. Hsu, Z. Wang, B. Kunert, C. Koos, and D. Van Thourhout, "Heterogeneous integration on silicon photonics," *Proc. IEEE*, vol. 106, no. 12, pp. 2258–2269, Dec. 2018.

[12] D. Liang et al., "Low-temperature, strong SiO$_2$-SiO$_2$ covalent wafer bonding for III-V compound semiconductors-to-silicon photonic integrated circuits," *J. Electron. Mater.*, vol. 37, no. 10, pp. 1552–1559, 2008.

[13] J. Zhang et al., "III-V-on-Si photonic integrated circuits realized using micro-transfer-printing," *APL Photon.*, vol. 4, no. 11, 2019, Art. no. 110803.

[14] S. Matsuo, T. Fujii, K. Hasebe, K. Takeda, T. Sato, and T. Kakitsuka, "Directly modulated buried heterostructure DFB laser on SiO$_2$/Si substrate fabricated by regrowth of InP using bonded active layer," *Opt. Exp.*, vol. 22, no. 10, pp. 12 139–12 147, 2014.

[15] Y. Hu et al., "III/V-on-Si MQW lasers by using a novel photonic integration method of regrowth on a bonding template," *Light Sci. Appl.*, vol. 8, no. 1, pp. 1–9, 2019.

[16] R. Jones et al., "Heterogeneously integrated InP/silicon photonics: Fabricating fully functional transceivers," *IEEE Nanotechnol. Mag.*, vol. 13, no. 2, pp. 17–26, Apr. 2019.

[17] V. Passaro, A. Cuccovillo, L. Vaiani, M. De Carlo, and C. E. Campanella, "Gyroscope technology and applications: A review in the industrial perspective," *Sensors*, vol. 17, no. 10, 2017, Art. no. 2284.

[18] J. K. Doylend and S. Gupta, "An overview of silicon photonics for LIDAR," in *Proc. SPIE 11285, Silicon Photon. XV*, Feb. 2020, Art. no. 112850J.

[19] N. Margalit, C. Xiang, S. M. Bowers, A. Bjorlin, R. Blum, and J. E. Bowers, "Perspective on the future of silicon photonics and electronics," *Appl. Phys. Lett.*, vol. 118, no. 22, 2021, Art. no. 220501.

[20] A. Y. Liu and J. Bowers, "Photonic integration with epitaxial III-V on silicon," *IEEE J. Sel. Topics Quantum Electron.*, vol. 24, no. 6, pp. 1–12, Nov./Dec. 2018.

[21] W. Jin, D. D. John, J. F. Bauters, T. Bosch, B. J. Thibeault, and J. E. Bowers, "Deuterated silicon dioxide for heterogeneous integration of ultra-low-loss waveguides," *Opt. Lett.*, vol. 45, no. 12, pp. 3340–3343, 2020.

[22] W. Jin, *Heterogeneous Integration Techniques for Ultra-Low Noise, Chip-Scale Lasers*. Santa Barbara, CA, USA: Univ. California, 2021.

[23] T. J. Kippenberg, A. L. Gaeta, M. Lipson, and M. L. Gorodetsky, "Dissipative Kerr solitons in optical microresonators," *Science*, vol. 361, no. 6402, Aug. 2018.

[24] M. A. Tran, D. Huang, and J. E. Bowers, "Tutorial on narrow linewidth tunable semiconductor lasers using Si/III-V heterogeneous integration," *APL Photon.*, vol. 4, no. 11, 2019, Art. no. 111101.

[25] B. Dahmani, L. Hollberg, and R. Drullinger, "Frequency stabilization of semiconductor lasers by resonant optical feedback," *Opt. Lett.*, vol. 12, no. 11, pp. 876–878, 1987.

[26] T. J. Kippenberg, R. Holzwarth, and S. A. Diddams, "Microresonator-based optical frequency combs," *Science*, vol. 332, no. 6029, pp. 555–559, 2011.

[27] M. A. Tran, D. Huang, T. Komljenovic, J. Peters, A. Malik, and J. E. Bowers, "Ultra-low-loss silicon waveguides for heterogeneously integrated silicon/III-V photonics," *Appl. Sci.*, vol. 8, no. 7, 2018, Art. no. 1139.

[28] J. F. Bauters et al., "Silicon on ultra-low-loss waveguide photonic integration platform," *Opt. Exp.*, vol. 21, no. 1, pp. 544–555, 2013.

[29] C. Xiang et al., "Laser soliton microcombs heterogeneously integrated on silicon," *Science*, vol. 373, no. 6550, pp. 99–103, 2021.

[30] P. A. Morton and M. J. Morton, "High-power, ultra-low noise hybrid lasers for microwave photonics and optical sensing," *J. Lightw. Technol.*, vol. 36, no. 21, pp. 5048–5057, 2018.

[31] D. Huang et al., "High-power sub-kHz linewidth lasers fully integrated on silicon," *Optica*, vol. 6, no. 6, pp. 745–752, 2019.

[32] C. Xiang, P. A. Morton, and J. E. Bowers, "Ultra-narrow linewidth laser based on a semiconductor gain chip and extended Si$_3$N$_4$ Bragg grating," *Opt. Lett.*, vol. 44, no. 15, pp. 3825–3828, 2019.

[33] T. Komljenovic, S. Srinivasan, E. Norberg, M. Davenport, G. Fish, and J. E. Bowers, "Widely tunable narrow-linewidth monolithically integrated external-cavity semiconductor lasers," *IEEE J. Sel. Topics Quantum Electron.*, vol. 21, no. 6, pp. 214–222, Nov./Dec. 2015, Art no. 1501909.

[34] P. Morton et al., "Integrated coherent tunable laser (ICTL) with 118 nm tuning range and sub-100 hz Lorentzian linewidth," in *Proc. Opt. Fiber Commun. Conf. Exhib.*, 2021, pp. 1–3.

[35] W. Bogaerts et al., "Silicon microring resonators," *Laser Photon. Rev.*, vol. 6, no. 1, pp. 47–73, 2012.

[36] M. A. Tran, D. Huang, J. Guo, T. Komljenovic, P. A. Morton, and J. E. Bowers, "Ring-resonator based widely-tunable narrow-linewidth Si/InP integrated lasers," *IEEE J. Sel. Topics Quantum Electron.*, vol. 26, no. 2, pp. 1–14, Mar./Apr. 2020.

[37] B. Liu, A. Shakouri, and J. E. Bowers, "Passive microring-resonator-coupled lasers," *Appl. Phys. Lett.*, vol. 79, no. 22, pp. 3561–3563, 2001.

[38] B. Liu, A. Shakouri, and J. Bowers, "Wide tunable double ring resonator coupled lasers," *IEEE Photon. Technol. Lett.*, vol. 14, no. 5, pp. 600–602, May 2002.

[39] C. Xiang et al., "Effects of nonlinear loss in high-Q Si ring resonators for narrow-linewidth III-V/Si heterogeneously integrated tunable lasers," *Opt. Exp.*, vol. 28, no. 14, pp. 19 926–19 936, 2020.

[40] K. Vahala and A. Yariv, "Detuned loading in coupled cavity semiconductor lasers-effect on quantum noise and dynamics," *Appl. Phys. Lett.*, vol. 45, no. 5, pp. 501–503, 1984.

[41] B. Stern, X. Ji, A. Dutt, and M. Lipson, "Compact narrow-linewidth integrated laser based on a low-loss silicon nitride ring resonator," *Opt. Lett.*, vol. 42, no. 21, pp. 4541–4544, 2017.

[42] Y. Fan et al., "Hybrid integrated InP-Si$_3$N$_4$ diode laser with a 40-Hz intrinsic linewidth," *Opt. Exp.*, vol. 28, no. 15, pp. 21 713–21 728, 2020.

[43] K. J. Boller et al., "Hybrid integrated semiconductor lasers with silicon nitride feedback circuits," *Photonics*, vol. 7, no. 4, 2020.

[44] J. Li, B. Zhang, S. Yang, H. Chen, and M. Chen, "Robust hybrid laser linewidth reduction using Si$_3$N$_4$-based subwavelength hole defect assisted microring reflector," *Photon. Res.*, vol. 9, no. 4, pp. 558–566, 2021.

[45] C. Xiang et al., "High-performance lasers for fully integrated silicon nitride photonics," *Nat. Commun.*, vol. 12, no. 1 pp. 1–8, 2021.

[46] C. O. de Beeck et al., "Heterogeneous III-V on silicon nitride amplifiers and lasers via microtransfer printing," *Optica*, vol. 7, no. 5, pp. 386–393, 2020.

[47] B. Jang et al., "A hybrid silicon evanescent quantum dot laser," *Appl. Phys. Exp.*, vol. 9, no. 9, 2016, Art. no. 0 92102.

[48] G. Kurczveil, D. Liang, M. Fiorentino, and R. G. Beausoleil, "Robust hybrid quantum dot laser for integrated silicon photonics," *Opt. Exp.*, vol. 24, no. 14, pp. 16 167–16 174, 2016.

[49] S. Uvin et al., "1.3 μm InAs/GaAs quantum dot DFB laser integrated on a Si waveguide circuit by means of adhesive die-to-wafer bonding," *Opt. Exp.*, vol. 26, no. 14, pp. 18 302–18 309, 2018.

[50] D. Liang et al., "High-performance quantum-dot distributed feedback laser on silicon for high-speed modulations," *Optica*, vol. 8, no. 5, pp. 591–593, 2021.

[51] Y. Wan et al., "High speed evanescent quantum-dot lasers on Si," *Laser Photon. Rev.*, vol. 15, no. 8, 2021, Art. no. 2100057.

[52] G. Kurczveil, M. A. Seyedi, D. Liang, M. Fiorentino, and R. G. Beausoleil, "Error-free operation in a hybrid-silicon quantum dot comb laser," *IEEE Photon. Technol. Lett.*, vol. 30, no. 1, pp. 71–74, Jan. 2018.

[53] C. Zhang, D. Liang, G. Kurczveil, A. Descos, and R. G. Beausoleil, "Hybrid quantum-dot microring laser on silicon," *Optica*, vol. 6, no. 9, pp. 1145–1151, 2019.

[54] A. Malik, J. Guo, M. A. Tran, G. Kurczveil, D. Liang, and J. E. Bowers, "Widely tunable, heterogeneously integrated quantum-dot o-band lasers on silicon," *Photon. Res.*, vol. 8, no. 10, pp. 1551–1557, 2020.

[55] S. Liu, M. Davenport, and J. E. Bowers, "Hybrid mode-locked 20 GHz colliding pulse Si/III-V laser with 890 fs pulsewidth," in *Proc. Conf. Lasers Electro- Opt.*, 2020, pp. 1–2.

[56] G. Kurczveil, C. Zhang, A. Descos, D. Liang, M. Fiorentino, and R. Beausoleil, "On-chip hybrid silicon quantum dot comb laser with 14 error-free channels," in *Proc. IEEE Int. Semicond. Laser Conf.*, 2018, pp. 1–2.

[57] B. R. Koch, A. W. Fang, O. Cohen, and J. E. Bowers, "Mode-locked silicon evanescent lasers," *Opt. Exp.*, vol. 15, no. 18, pp. 11 225–11 233, 2007.

[58] M. L. Davenport, S. Liu, and J. E. Bowers, "Integrated heterogeneous silicon/III-V mode-locked lasers," *Photon. Res.*, vol. 6, no. 5, pp. 468–478, 2018.

[59] P. Del'Haye, A. Schliesser, O. Arcizet, T. Wilken, R. Holzwarth, and T. J. Kippenberg, "Optical frequency comb generation from a monolithic microresonator," *Nature*, vol. 450, no. 7173, pp. 1214–1217, 2007.

[60] J. S. Levy, A. Gondarenko, M. A. Foster, A. C. Turner-Foster, A. L. Gaeta, and M. Lipson, "CMOS-compatible multiple-wavelength oscillator for on-chip optical interconnects," *Nature Photon.*, vol. 4, no. 1, pp. 37–40, 2010.

[61] X. Ji et al., "Ultra-low-loss on-chip resonators with sub-milliwatt parametric oscillation threshold," *Optica*, vol. 4, no. 6, pp. 619–624, 2017.

[62] J. Liu et al., "Ultralow-power chip-based soliton microcombs for photonic integration," *Optica*, vol. 5, no. 10, pp. 1347–1353, 2018.

[63] Y. He et al., "Self-starting Bi-chromatic LiNbO3 soliton microcomb," *Optica*, vol. 6, no. 9, pp. 1138–1144, 2019.

[64] C. Wang, M. Zhang, M. Yu, R. Zhu, H. Hu, and M. Loncar, "Monolithic lithium niobate photonic circuits for kerr frequency comb generation and modulation," *Nature Commun.*, vol. 10, no. 1, pp. 1–6, 2019.

[65] L. Chang et al., "Ultra-efficient frequency comb generation in AlGaAs-on-insulator microresonators," *Nature Commun.*, vol. 11, no. 1, pp. 1–8, 2020.

[66] D. M. Lukin et al., "4h-silicon-carbide-on-insulator for integrated quantum and nonlinear photonics," *Nature Photon.*, vol. 14, no. 5, pp. 330–334, 2020.

[67] A. Malik et al., "Low power consumption silicon photonics datacenter interconnects enabled by a parallel architecture," in *Proc. Opt. Fiber Commun. Conf. Exhib.*, 2021, pp. 1–3.

[68] Z. Zhang, J. C. Norman, S. Liu, A. Malik, and J. E. Bowers, "Integrated dispersion compensated mode-locked quantum dot laser," *Photon. Res.*, vol. 8, no. 9, pp. 1428–1434, 2020.

[69] K. Van Gasse et al., "Recent advances in the photonic integration of mode-locked laser diodes," *IEEE Photon. Technol. Lett.*, vol. 31, no. 23, pp. 1870–1873, Dec. 2019.

[70] Z. Wang et al., "A III-V-on-Si ultra-dense comb laser," *Light Sci. Appl.*, vol. 6, no. 5, pp. e16260–e16260, 2017.

[71] S. Cuyvers et al., "Low noise heterogeneous III-V-on-silicon-nitride mode-locked comb laser," *Laser Photon. Rev.*, vol. 15, no. 8, 2021, Art. no. 2000485.

[72] S. Liu et al., "High-channel-count 20 GHz passively mode-locked quantum dot laser directly grown on Si with 4.1 Tbit/s transmission capacity," *Optica*, vol. 6, no. 2, pp. 128–134, 2019.

[73] B. Braun, K. Weingarten, F. Kärtner, and U. Keller, "Continuous-wave mode-locked solid-state lasers with enhanced spatial hole burning," *Appl. Phys. B*, vol. 61, pp. 429–437, 1995.

[74] A. L. Gaeta, M. Lipson, and T. J. Kippenberg, "Photonic-chip-based frequency combs," *Nature Photon.*, vol. 13, no. 3, pp. 158–169, 2019.

[75] N. Pavlov et al., "Narrow-linewidth lasing and soliton kerr microcombs with ordinary laser diodes," *Nature Photon.*, vol. 12, no. 11, pp. 694–698, 2018.

[76] B. Shen et al., "Integrated turnkey soliton microcombs," *Nature*, vol. 582, no. 7812, pp. 365–369, 2020.

[77] W. Xie et al., "Heterogeneous silicon photonics sensing for autonomous cars," *Opt. Exp.*, vol. 27, no. 3, pp. 3642–3663, 2019.

[78] R. Blum, "Integrated silicon photonics for high-volume data center applications," *Proc. SPIE*, vol. 11286, Feb. 2020, Art. no. 112860M.

[79] J. Sun, R. Kumar, M. Sakib, J. B. Driscoll, H. Jayatilleka, and H. Rong, "A 128 Gb/s PAM4 silicon microring modulator with integrated thermo-optic resonance tuning," *J. Lightw. Technol.*, vol. 37, no. 1, pp. 110–115, 2019.

[80] M. Sakib et al., "A high-speed micro-ring modulator for next generation energy-efficient optical networks beyond 100Gbaud," in *Proc. Conf. Lasers Electro- Opt.*, 2021, Art. no. SF1C.3.

[81] H. Li et al., "A 112 Gb/s PAM4 silicon photonics transmitter with microring modulator and CMOS driver," *J. Lightw. Technol.*, vol. 38, no. 1, pp. 131–138, 2020.

[82] S. Fathololoumi et al., "1.6 Tbps silicon photonics integrated circuit and 800 Gbps photonic engine for switch co-packaging demonstration," *J. Lightw. Technol.*, vol. 39, no. 4, pp. 1155–1161, 2021.

[83] H. Li et al., "A 4x50 Gb/s all-silicon ring-based WDM transceiver with CMOS IC," in *Proc. Eur. Conf. Opt. Commun.*, 2021, Art. no. We4G.3.

[84] S. Pitris et al., "400 Gb/s silicon photonic transmitter and routing WDM technologies for glueless 8-socket chip-to-chip interconnects," *J. Lightw. Technol.*, vol. 38, no. 13, pp. 3366–3375, 2020.

[85] M. Wade et al., "An error-free 1Tbps WDM optical I/O chiplet and multi-wavelength multi-port laser," in *Proc. Opt. Fiber Commun. Conf.*, 2021, Art. no. F3C.6.

[86] R. Jones, "Overview and future challenges on III-V integration technologies in silicon photonics platform," in *Proc. Opt. Fiber Commun. Conf.*, 2021, Art. no. M5A.1.

[87] H. Jayatilleka et al., "Post-fabrication trimming of silicon photonic ring resonators at wafer-scale," *J. Lightw. Technol.*, vol. 39, no. 15, pp. 5083–5088, 2021.

[88] P. Liao et al., "A 260 Gb/s/lambda link with silicon photonic dual-polarization transmitter and polarization demultiplexer," in *Proc. Eur. Conf. Opt. Commun.*, 2021, Art. no. Tu4D.1.

[89] C. R. Doerr, N. K. Fontaine, and L. L. Buhl, "PDM-DQPSK silicon receiver with integrated monitor and minimum number of controls," *IEEE Photon. Technol. Lett.*, vol. 24, no. 8, pp. 697–699, Apr. 2012.

[90] D. J. Blumenthal, "Photonic integration for UV to IR applications," *APL Photon.*, vol. 5, no. 2, 2020, Art. no. 0 20903.

[91] G. Roelkens et al., "III-V-on-silicon photonic devices for optical communication and sensing," *Photonics*, vol. 2, no. 3, pp. 969–1004, 2015.

[92] T. Hu et al., "Silicon photonic platforms for mid-infrared applications," *Photon. Res.*, vol. 5, no. 5, pp. 417–430, 2017.

[93] R. Soref, "Mid-infrared photonics in silicon and germanium," *Nature Photon.*, vol. 4, no. 8, pp. 495–497, 2010.

[94] T. Kamei, T. Kamikawa, M. Araki, S. P. DenBaars, S. Nakamura, and J. E. Bowers, "Research toward a heterogeneously integrated InGaN laser on silicon," *Physica Status Solidi (A)*, vol. 217, no. 7, 2020, Art. no. 1900770.

[95] T. J. Morin et al., "CMOS-foundry-based blue and violet photonics," *Optica*, vol. 8, no. 5, pp. 755–756, 2021.

[96] A. Spott et al., "Quantum cascade laser on silicon," *Optica*, vol. 3, no. 5, pp. 545–551, 2016.

[97] A. Malik et al., "Integration of mid-infrared light sources on silicon-based waveguide platforms in 3.5–4.7 μm wavelength range," *IEEE J. Sel. Topics Quantum Electron.*, vol. 25, no. 6, Nov./Dec. 2019, Art. no. 1502809.

[98] J. Chiles and S. Fathpour, "Mid-infrared integrated waveguide modulators based on silicon-on-lithium-niobate photonics," *Optica*, vol. 1, no. 5, pp. 350–355, 2014.

[99] R. Wang et al., "2 μm wavelength range inp-based type-ii quantum well photodiodes heterogeneously integrated on silicon photonic integrated circuits," *Opt. Exp.*, vol. 23, no. 20, pp. 26 834–26 841, 2015.

[100] S. Yamaoka et al., "Directly modulated membrane lasers with 108 GHz bandwidth on a high-thermal-conductivity silicon carbide substrate," *Nature Photon.*, vol. 15, no. 1, pp. 28–35, 2021.

[101] T. Hiraki et al., "Heterogeneously integrated III-V/Si MOS capacitor mach-zehnder modulator," *Nature Photon.*, vol. 11, no. 8, pp. 482–485, 2017.

[102] J.-H. Han, F. Boeuf, J. Fujikata, S. Takahashi, S. Takagi, and M. Takenaka, "Efficient low-loss InGaAsP/Si hybrid MOS optical modulator," *Nature Photon.*, vol. 11, no. 8, pp. 486–490, 2017.

[103] B. Tossoun et al., "Indium arsenide quantum dot waveguide photodiodes heterogeneously integrated on silicon," *Optica*, vol. 6, no. 10, pp. 1277–1281, 2019.

[104] J. Wang, F. Sciarrino, A. Laing, and M. G. Thompson, "Integrated photonic quantum technologies," *Nature Photon.*, vol. 14, no. 5, pp. 273–284, 2020.

[105] B. J. Shastri et al., "Photonics for artificial intelligence and neuromorphic computing," *Nature Photon.*, vol. 15, no. 2, pp. 102–114, 2021.

[106] R. Won, "Integrating silicon photonics," *Nature Photon.*, vol. 4, no. 8, pp. 498–499, 2010.

Chao Xiang (Member, IEEE) received the B.E. degree in optoelectronic information engineering from the Huazhong University of Science and Technology, Wuhan, China, the M.Phil. degree in information engineering from the Chinese University of Hong Kong, Hong Kong, and the Ph.D. degree from the Department of Electrical and Computer Engineering, University of California, Santa Barbara, Santa Barbara, CA, USA. He is currently a Postdoctoral Scholar with the University of California, Santa Barbara. His research interests include semiconductor lasers, silicon photonics, integrated nonlinear photonics, and heterogeneous photonic integrated circuits.

Warren Jin received the B.S. degree in computer engineering from Brown University, Providence, RI, USA. He is currently working toward the Ph.D. degree with the Electrical Engineering Department, University of California, Santa Barbara, Santa Barbara, CA, USA. His research interests include silicon photonics, and applications of piezoelectrics and MEMS in photonic integrated circuits.

Duanni Huang (Member, IEEE) received the B.S. degree in electrical engineering from the Massachusetts Institute of Technology, Cambridge, MA, USA, in 2013, and the M.S. and Ph.D. degrees in electrical engineering from the University of California, Santa Barbara, CA, USA, in 2015 and 2019, respectively. He is currently a Research Scientist with Intel Labs, working on silicon photonics with an emphasis on heterogeneous integration.

Minh A. Tran (Member, IEEE) received the B.S. degree in electrical engineering from the University of Tokyo, Tokyo, Japan, in 2013, and the M.S. and Ph.D. degrees in electrical engineering from the University of California, Santa Barbara, Santa Barbara, CA, USA, in 2015 and 2018, respectively. He is currently with Nexus Photonics, a startup company based in Goleta, CA, USA.

Joel Guo received the B.S. degree in electrical engineering from the University of Texas at Austin, Austin, TX, USA, in 2018, and the M.S. degree in 2020 in electrical engineering from the University of California, Santa Barbara, CA, USA, where he is currently working toward the Ph.D. degree. His research interests include heterogeneous narrow linewidth lasers and photonic integrated circuits.

Yating Wan received the Ph.D. degree from the Department of Electrical and Computer Engineering, Hong Kong University of Science and Technology, Hong Kong, in 2017. Then he joined the Prof. John Bowers' Group, University of California Santa Barbara, Santa Barbara, CA, USA, as a Postdoctoral Research Associate. Her research interests include microcavity quantum dot optoelectronics and silicon photonics. She had been awarded the 2016–2017 HKUST Ph.D. Research Excellence Award, 2021 CLEO Tingye Li Innovation Prize, 2018 PIERS Young Scientist Award, 2018 Rising Stars Women in Engineering Asia, and 2020 Rising Stars 2020 Women in EECS.

Weiqiang Xie received the bachelor's degree in applied physics from Xi'an Jiaotong University, Xi'an, China, in 2008, and the master's degree in condensed matter physics from Shanghai Jiao Tong University, Shanghai, China, in 2011. Then he joined Photonics Research Group, Ghent University, Ghent, Belgium, and received the Ph.D. degree in photonics engineering in 2016. From 2017 to 2021, he was a Postdoctoral Researcher of heterogeneous photonics integration with the University of California, Santa Barbara, Santa Barbara, CA, USA. He is currently an Associate Professor with Shanghai Jiao Tong University. His research interests include silicon, silicon nitride photonics and their heterogeneous integration with novel materials (III-V, quantum dots, etc). His research interests include applications such as telecom, optical interconnect, and sensing.

Geza Kurczveil (Member, IEEE) received the Ph.D. degree in electrical and computer engineering from the University of California, Santa Barbara, CA, USA, in 2012, working on optical buffers. He is currently a Research Scientist with Hewlett Packard Labs, Palo Alto, CA, USA. He has authored or coauthored more than 50 journal and conference papers. His current research interests include silicon photonic integrated circuits and nano-photonics.

Andrew M. Netherton received the B.S. degree in electrical engineering from the University of Illinois at Urbana-Champaign, Champaign, IL, USA, in 2016, and the M.S. degree in 2018 in electrical and computer engineering from the University of California Santa Barbara, Santa Barbara, CA, USA, where he is currently working toward the Ph.D. degree in electrical and computer engineering. His research interests include silicon photonics and energy efficient datacenter communication links.

Di Liang (Senior Member, IEEE) is currently a Distinguished Technologist and Research Manager with Hewlett Packard Labs, Hewlett Packard Enterprise. He has authored and coauthored more than 250 journal and conference papers, six book chapters, and was granted by 45 patents with another more than 55 pending. His research interests include III-V and silicon photonics and heterogeneous material integration. He is an Associate Editor for the IEEE JOURNAL OF QUANTUM ELECTRONICS and *OSA Photonics Research*. He is a Fellow of OSA and a Member of SPIE.

Haisheng Rong (Senior Member, IEEE) received the B.Sc. and M.Sc. degrees from Nankai University, Tianjin, China, and the Ph.D. degree from the University of Heidelberg, Heidelberg, Germany. He is currently a Senior Principal Engineer with Intel Labs. He has made numerous contributions to the development and commercialization of silicon photonics technology with Intel. He was the recipient of the Intel Achievement Award and Intel Labs Academy Award for his outstanding achievements. He is the Winner the Scientific American 50 Award for his work on the development of silicon-based lasers in 2005 and is a Key Member of the Intel Team winning the Paul F. Forman Team Engineering Excellence Award in 2014. He is a Fellow of OSA.

John E. Bowers (Fellow, IEEE) received the M.S. and Ph.D. degrees from Stanford University, Stanford, CA, USA. He was with AT&T Bell Laboratories before joining the University of California Santa Barbara, Santa Barbara, CA, USA. He is the Director of the Institute for Energy Efficiency and a Professor with the Department of Electrical and Computer Engineering and Materials, University of California, Santa Barbara. His research interests include primarily concerned with silicon photonics, optoelectronic devices, optical switching and transparent optical networks and quantum dot lasers. He is a Fellow of the OSA and the American Physical Society, and the recipient of the IEEE Photonics Award, OSA/IEEE Tyndall Award, the IEEE LEOS William Streifer Award, and the South Coast Business and Technology Entrepreneur of the Year Award. He is a Member of the National Academy of Engineering and National Academy of Inventors.